Methods

Sample construction

The majority of our experiments were conducted using PMMA blocks of dimensions 200x6x100mm (top block) and 300x30x28mm (base block) in the *x*, *y*, and *z* directions respectively. The contact face of the top blocks were diamond machined to a roughness of approximately 1μm (r.m.s). The bottom blocks were also roughened to ~1μm (r.m.s). Wave velocities were measured using "time of flight" of acoustic pulses providing shear and longitudinal velocities of c_s = 1370 ± 50 m/s, and c_l = 2730 ± 50 m/s. These yield the Rayleigh wave speed, c_R = 1280 ± 40m/s *(1)*. We checked the independence of the durations of Phases II and III on sample geometry by doubling the height and width of the base block and by varying *X* from 10 to 70mm. No effect was observed.

Experimental Setup

A schematic depiction of the experimental setup is given in Figure S1. At the beginning of each experiment a spatially uniform normal loading, F_N, was applied to the top block and was continuously measured via a load cell. Shear loading, F_S, was applied to system as follows. The base block, was mounted on a low friction linear stage. Its motion was only constrained by the frictional coupling to the slider via the contact interface.

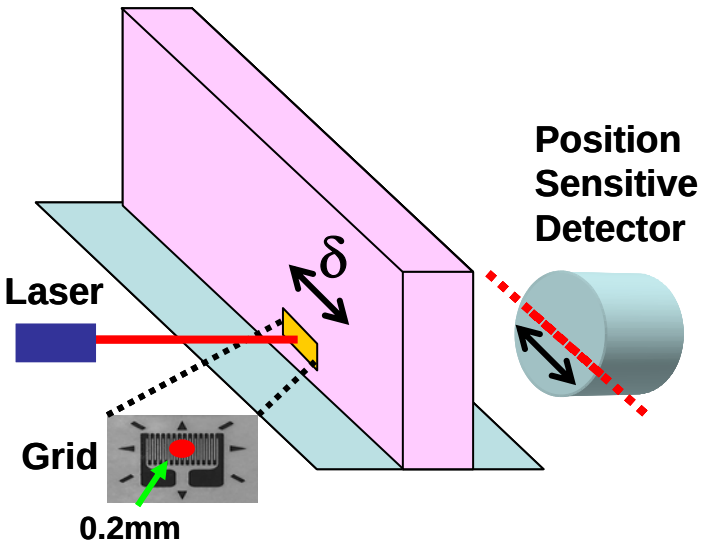

Figure S1: Experimental set up

Shear was applied to the system via an S-Beam load cell (which measured F_S) of stiffness 10^7 N/m, which was sandwiched between the low friction stage and a rigid linear actuator. The linear actuator applied shear to the system by advancing at a constant displacement rate of 8μm/sec while compressing the load cell. A rigid stopper, set at height *h* above the interface plane, was applied to the slider's trailing edge at x=0, to constrain its motion. Slip in the system initiated at $x=0$ and advanced in the positive x direction along the interface plane. Throughout the experiments a Philtec D20 optical displacement sensor was used to monitor slip at the top block's leading edge (x=200mm) to better than 0.5μm accuracy at a measurement rate of 250,000 sample/sec.

Figure S1 describes our method of measuring the local slip, $\delta(t)$, at a location, X, adjacent to the interface. A laser beam was focused to a spot size ~0.2mm and passed through a thin metallic grid that was glued to the side of the top block, approximately 2mm above the frictional interface. The spacing between grid lines was 0.07mm. The diffraction pattern through the grid was incident on a position sensitive detector (PSD) positioned a distance of 60-70cm from the interface. The output voltage of the amplified PSD system was proportional to the distance of the "center of mass" of the diffraction pattern from the center of the detector. This method enables slip measurements with an accuracy of ~0.2μm at acquisition rates of up to 1MHz. Since the leading edge of the top block did not slip during the course of these experiments, measurements of its motion were subtracted from the slip measurements at X to remove noise due to overall system vibrations from the local slip measurements.

The full details of the real contact area, $A(x,t)$, measurement method were given elsewhere *(2)*. The interface area was illuminated via a sheet of laser light whose incident angle was well beyond the angle for total internal reflection from the interface. Images of the entire sample length were taken using a Full Camera Link NI-1429 frame grabber in conjunction with a VDS CMC-1300/485N fast camera capable of capturing 250,000 single line images (1280 x 1 pixels) per second (temporal resolution of 4μsec). Since the spacing between contact points ranges between 2-10μm, each pixel of the camera is mapped to a (x × y) 0.2mm × 0.8 mm region of the interface that comprises thousands of individual contacts. At each point, the real contact area is a linear function of the local normal load. For the range of applied normal loads, the transmitted light intensity I at a point is, to a good approximation, a linear function of A for small

changes of the normal loading. However, evanescent light introduces some curvature to the I as function of A relation. To account for this, a quasistatic calibration of I to F_N was performed prior to each experiment, where the local value of F_N at each location X was measured by means of a miniature strain-gage (Vishay 031 MF) mounted on the top block, adjacent to the interface.

Slow (25Hz) measurements of all the measured quantities were taken continually throughout the entire run. Rapid acquisition was triggered by means of an acoustic transducer mounted on the trailing edge (x=0) of the top block. Thus, a complete record was obtained spanning measurement timescales from μsec to hundreds of seconds. The triggering signal was also used to halt the shear loading and fix F_S throughout a pre-set measurement period ranging from 5-100 sec. After this period, the loading was resumed.

Determination of aging coefficients

The time of slip arrest, t_0, was determined from the slip measurements. β was obtained by fitting the data at long times, when $A(t)$ varies logarithmically, to the form $A(t)/A(t_0) = p+\beta\cdot\log(t)$ which is linear in its logarithmic argument. $A(t_0)$ was evaluated as the value of the plateau at the final stages of Phase III. Equation 1 reduces to $A(t)/A(t_0) = 1+\beta\cdot\log(t)-\beta\cdot\log(\tau)$ for times much larger than τ and t_0. Equating these two forms of $A(t)/A(t_0)$ at large times, we obtained $\tau = exp[(1-p)/\beta]$. Typical confidence bounds for this evaluation procedure (error bars in Figure 3c) reflect the cumulative error of this fitting process.

Calculations of thermal cooling time, t_{cool}

Here, we estimate the cooling time, t_{cool}, that defines the duration of Phase II. t_{cool} is the time needed for the layer heated by fracture to cool to below the glass temperature, T_g (~110˚C). Let us assume that the fracture energy is instantaneously deposited within a thin uniform layer of thickness h between $z = \pm h/2$. This results in a uniform temperature increase of $\Delta T \sim \Gamma/(\rho C_P\cdot h)$ where Γ, ρ, C_P are, respectively, the fracture energy, density (1190kg/m^3), and heat capacity (1490 J/(kg·˚C)) of PMMA. The cooling of this layer is governed by the 1D heat diffusion equation whose solution at the interface (z=0) in terms of the error function, *erf*, is:

$$T(t) - T_{room} = -\frac{\Gamma}{4\rho C_P h}\left[erf\left(\frac{-h}{\sqrt{4\chi t}}\right) - erf\left(\frac{h}{\sqrt{4\chi t}}\right)\right] \qquad \text{(S1)}.$$

where χ=1.1 × 10^{-7}m^2/sec is the thermal diffusivity of PMMA. χ, ρ, and C_P are well-known for PMMA. The value of Γ is, however, unknown for this process.

We may estimate the value of Γ by using the measured value *(3)* of Γ ~ 1000-2000J/m^2 for the tensile fracture of PMMA. This estimate is roughly justified as follows. Any plastic deformation of interlocking asperities enabling motion should be similar to the stress-induced plastic deformation that takes place in Mode I fracture, which is the main contributor to the fracture energy of PMMA in tensile fracture. In tensile fracture, these processes occur within a dissipative zone ("process zone") whose 1μm scale is similar to our interface thickness. Thus, as the same deformation processes take place over a similar scale, we might expect a similar value of Γ. With this value, Equation (S1) yields cooling times between 30μsec < t_{cool} < 120μsec for $h \lesssim 1\mu$m. These values are compatible with the 60 μsec measured duration of Phase II and are only weakly dependent on h.

[1] Landau & Lifshitz, "Theory of Elasticity" 3rd Edition, section 24, pg. 96.

[2] S. M. Rubinstein, M. Shay, G. Cohen, J. Fineberg Int. J. of Fracture **140,**212-201 (2006).

[3] E. Sharon, J. Fineberg, *Nature* **397**, 333-335 (1999).